Colloids and Surfaces A: Physicochemical and Engineering Aspects 648 (2022) 129217

Contents lists available at ScienceDirect

Colloids and Surfaces A: Physicochemical and Engineering Aspects

journal homepage: www.elsevier.com/locate/colsurfa

Single-step functionalization of silicon nanoparticles providing efficient DNA binding

Paul Cannon [a], Brian Freeland [b], Margaux Jaquiery [b], Enda McGlynn [c], Jennifer Gaughran [a,*]

[a] School of Physical Sciences, Dublin City University, Dublin 9, Ireland
[b] School of Biotechnology, Dublin City University, Dublin 9, Ireland
[c] School of Physical Sciences and NCPST, Dublin City University, Dublin 9, Ireland

HIGHLIGHTS

- A recirculatory flow configuration of pulsed laser ablation in liquids was demonstrated.
- Higher functionalization efficiencies and nanoparticle concentrations were obtained compared to previously established flow set-ups.
- 100% functionalization efficiency is achievable for nucleic acids with low-cost, biocompatible silicon nanoparticles.

GRAPHICAL ABSTRACT

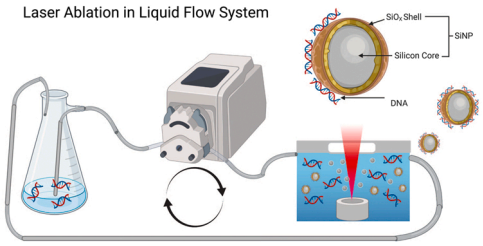

ARTICLE INFO

Keywords:
Silicon nanoparticles
DNA
Pulsed laser ablation in liquids
Recirculating flow
Functionalization
Disease detection

ABSTRACT

Hypothesis: Functionalized nanoparticles (NPs) offer diverse biomedical applications, but their synthesis is complex, costly, and labour-intensive, particularly when providing for additional functionalization requirements which are a key feature of biomedical applications. Pulsed laser ablation in liquids (PLAL) has previously allowed for the synthesis of metal and metal oxide nanoparticles using metal targets, which can then be surface functionalized during synthesis by the surrounding liquid species. Therefore, it should be possible to achieve biomolecule functionalization by ablating in biomolecular solutions. We explore a novel controlled recirculation PLAL scheme which should increase functionalization and productivity of functionalized nanoparticles.
Experiments: Traditional PLAL was performed by ablating a silicon target in a DNA solution. We have extended beyond traditional approaches by ablating the silicon target under novel flow conditions in a controlled recirculating loop of DNA solution.
Findings: Ablating in a DNA solution allows for high efficiency binding of DNA to silicon nanoparticles (SiNPs) in a single step process. By using SiNPs we are significantly reducing the overall cost of the process, when compared with the more traditional use of gold or silver; as well as, using a biocompatible material with an affinity for protein and nucleic acid binding. Reducing the laser shielding effects of particles and debris by removing them from the ablation site produces higher volumes and concentrations of functionalized colloid. Recirculating this liquid over the target has resulted in a 50% relative increase in binding efficiency, compared with static and single-pass flow conditions processing, achieving an average maximum binding efficiency of 78% in flow compared to 52% under static conditions. Furthermore, by reducing the initial DNA concentration, we were able to achieve 100% binding efficiency, which we believe to be the highest reported in literature to date.

* Corresponding author.
E-mail address: jennifer.gaughran@dcu.ie (J. Gaughran).

https://doi.org/10.1016/j.colsurfa.2022.129217
Received 7 January 2022; Received in revised form 7 May 2022; Accepted 10 May 2022
Available online 13 May 2022
0927-7757/© 2022 The Authors. Published by Elsevier B.V. This is an open access article under the CC BY-NC-ND license (http://creativecommons.org/licenses/by-nc-nd/4.0/).

1. Introduction

Nucleic acid testing offers the capability for early detection of diseases, but their capture can be a lengthy and difficult process [1]. The COVID-19 pandemic has further highlighted the need for faster diagnostic tools, as diagnosis is based on the detection of viral nucleic acids via polymerase chain reaction (PCR) [2]. The complexity of the technique requires localized testing centers to be set up worldwide to accommodate the specialized personnel, equipment and reagents needed. As the healthcare industry moves towards a point-of-care approach, we need to look at the miniaturization of DNA diagnostic techniques which presents quite a challenge [1,3]. The use of nanoparticles (NPs) may offer a solution to this challenge. In recent years, DNA-NP conjugates have been developed which can overcome these difficulties [4]. The capabilities of these conjugates are not just restricted to nucleic acid testing, but offer a diverse array of uses such as drug delivery [5,6], therapeutic agents [7], multipurpose biosensors [8], and cellular imaging [9]. DNA-NP conjugates are highly diverse due to the various physicochemical properties that different nanomaterials have, as well as the properties imparted by the chosen synthesis method [10]. However, the conjugation processes often involves many lengthy steps, typically including the coupling of oligonucleotides through thermal thiol groups to colloidal NPs, which is resource- and time-intensive [11,12]. Also, the NP fabrication techniques need to be considered, as many use environmentally harmful solvents/reagents [13,14] which result in undesirable precursors/stabilizers on the surface of the NPs which must then be removed in order to functionalize them.

Pulsed laser ablation in liquids (PLAL) is a green method for the synthesis of ligand-free NPs [15]. It is a cost-, labor-, and time-efficient technique that does not require chemicals that potentially inhibit subsequent reactions [16,17]. PLAL involves immersing a solid target in a solvent and irradiating it with a high intensity pulsed laser. The laser radiation vaporizes the solid surface structure and surrounding liquid environment, creating an oscillating cavitation bubble [18,15]. The oscillation within the highly confined conditions and subsequent induced high-pressure of the cavitation bubble by the surrounding liquid causes the ablated matter to nucleate and agglomerate, forming NPs. This nucleation site then acts as a growing center for the adsorption of species within the liquid [19]. This technique is capable of a high degree of customization and control, as NP morphology can be precisely controlled by altering the various process parameters such as the liquid solvent and laser wavelength, power, and repetition rate [20]. In this study, we ablated a silicon target in a DNA solution to create SiNPs with a DNA functionalized surface, using double stranded DNA as a model biomarker for functionalization. By ablating directly in a DNA solution, in addition to the increased binding efficiency via in-situ functionalization, we also increase the scalability of this technique by lowering the number of steps required to produce these functionalized nanoparticles.

While PLAL has proven itself as a desirable NP synthesis method [15], it is typically done under static flow conditions, i.e., the target material is ablated in an undisturbed petri dish or beaker filled with liquid. This is a very simple technique to perform, but it is quite inefficient with low NP productivity. In this work, we build upon the flow ablation process developed by Streubel et al. [21] and Waag et al. [22], while using both the flow-cell design and recirculation configuration reported by Freeland et al. [23,14], to recirculate liquid over the target in a controlled manner to create a novel enhanced PLAL system. In doing so, the SiNPs are directed away from the ablation site, reducing the laser shielding effects created by the produced NPs, and allowing for significantly larger colloid production volumes and concentrations. The recirculation provides longer DNA-SiNP interaction time, at the site of NP creation, under enhanced mixing conditions to further promote binding.

While metal and heavy-metal nanoparticles are more commonly used during PLAL, these materials exhibit unpredictable biotoxicity and can damage proteins and nucleic acids, making them unsuitable for in-vivo applications [24,25]. However, SiNPs present an attractive and viable platform for biological applications [26,27] due to their biocompatibility and the well-established affinity of silicon surfaces for protein and nucleic acid adsorption [28]. This relationship between silicon surfaces and nucleic acids forms the foundation of the current state-of-the-art method for the solid-phase purification of DNA [29], and is used to prepare crude samples for PCR analysis.

The use of the novel controlled recirculation system has allowed us to achieve successful synthesis of SiNPs and attain a 50% relative increase in binding efficiency, compared with static and single-pass flow conditions processing, achieving an average maximum binding efficiency of 78% in flow compared to 52% under static conditions, and up to 100% efficiency in a solution with reduced DNA concentrations, which is the highest reported value to date to our knowledge.

2. Materials & methods

2.1. Synthesis & functionalization

Schematic diagrams of the four ablation setups used in our study are shown in Fig. 1. Laser parameters were previously optimized for SiNP generation from a silicon target [99.999% metal basis, Alfa Aesar] submerged in a liquid using a low-power micro-machining Nd: YAG laser [WEDGE HF 1064, Bright Solutions, Italy] ($\lambda = 1064$ nm, $\tau_p = 100$ ns, $f_{rep} = 10{,}000$ Hz, $F = 1.83$ J/cm^2) [30]. The beam was focused on the target, and raster scanned across the silicon surface at a speed of 2 mm/s, moving in an Archimedean spiral, using a 2D scanning galvanometer [Raylase SS-12]. This scanning process achieves a more uniform and efficient ablation compared to the cratering that occurs during stationary irradiation, and reduces the re-irradiation of previously generated NPs, which can create size heterogeneity and further reduce production efficiency [31]. The target was maintained within the beam-waist using an M404 4PD 1-D nanopositioning stage [PI, Germany], controlling the spot size at 100 μm in diameter. The beam profile is Gaussian, exhibiting a near TEM_{00} mode (ellipticity 0.97) using an F-theta lens.

The first method investigated was a two-step ex-situ binding (Fig. 1.a). This involved ablating silicon in 11 mL of an ionic buffer solution [Qiagen PB binding buffer] for 20 min and mixing the SiNP colloid with DNA for approximately 10 s post-ablation.

For static in-situ functionalization (Fig. 1.b), the silicon target was placed in a petri dish and submerged in 11 mL of the ionic buffer solution containing 2, 20 or 100 μg/mL DNA [Sigma Aldrich Deoxyribonucleic acid sodium salt from calf thymus] and ablated for 20 min. We utilized calf thymus DNA for this investigation, which is a widely used strain for DNA binding studies [32,33].

Single-pass (non-recirculatory) flow ablations were performed using the setup shown in Fig. 1.c. Using the design reported by Freeland et al. a 3D-printed flow cell was custom-designed such that the liquid flow is laminar, thereby removing occluding bubbles, particles, and debris and maintaining ablation efficiency. A reservoir was filled with 2 μg/mL DNA solution and a peristaltic pump [Isamatic MCPV510 with Millipore XX80EL005 head] passes the fluid around the tubing network [polytetrafluoroethylene tubes, total volume 22.5 mL] and into a collection beaker on the opposite end of the flow cell at three different flow rates (40, 85, and 135 mL/min]. Initially, the liquid was allowed to flow into a waste chamber for up to 10 s (this varied depending on the flow rate) before being directed into the new beaker. This was to ensure that only DNA-SiNP colloid was being captured instead of the pure DNA solution used to prime the flow system prior to ablation. Contrary to the other methods discussed, the single-pass was not performed for a specific time but rather 40 mL of DNA solution was placed in the reservoir, and the test was stopped after the reservoir was emptied. 15 mL was used to prime the system and the working volume was 25 mL. Considering the higher flow rates would require liters of DNA solution for a single test, and we performed multiple repeat tests, we opted to use the same

volume of DNA solution as the recirculatory ablation method discussed below. As the SiNP concentrations during the single-pass method are time independent, we believe this to be an approach enabling comparisons with other methods.

Controlled recirculatory flow ablations (Fig. 1.d) utilized the same setup as Fig. 1.c; however, the outlet tubing was placed back into the initial DNA reservoir rather than into a separate collection beaker. Here. 25 mL of the same DNA solution is circulated over the target multiple times in a closed loop at a constant flow rate of 135 mL/min for varying ablation times (5, 10, 20, 40, and 60 min).

All samples were allowed to settle for a 12–16-h period prior to centrifugation and binding analysis.

2.2. SiNP characterization

Size and morphology of SiNPs produced were characterized via Dynamic Light Scattering spectroscopy (DLS) [NANO-flex® 180° DLS Size, Microtrac Ltd] and Transmission Electron Microscope (TEM) imaging [FEI]. TEM was performed using BioTwin lens with a 120 kV LaB6 emitter at 3 Å resolution limit and a Veleta 2048 × 2048 wide angle detector. Samples were prepared using a copper mesh TEM grid with 40 μL of sample applied and allowed to evaporate at room temperature.

The chemical and crystallographic properties of the produced particles were characterized using Energy Dispersive X-Ray Spectroscopy (EDX) [Oxford Instruments Xplore detector mounted in a Karl-Zeiss EVO 50 series scanning electron microscope], Fourier Transform Infrared Spectroscopy (FTIR) [PerkinElmer Spectrum Two FT-IR], and X-Ray Diffraction (XRD) [Bruker AXS D8 Advance Texture Diffractometer]. For EDX and XRD, 100 μL of SiNPs in concentrations ranging from 3 to 8 mg/mL were pipetted onto silicon-carbide substrates (4H-SiC) and allowed to dry at room temperature. This was repeated 10–15 times to achieve an appropriately thick coating for each analysis. EDX spectra were obtained for an incident 5 keV electron beam. FTIR was performed by pipetting the same solutions onto the attenuated total reflection attachment of the system. FTIR spectra were corrected for air, but the

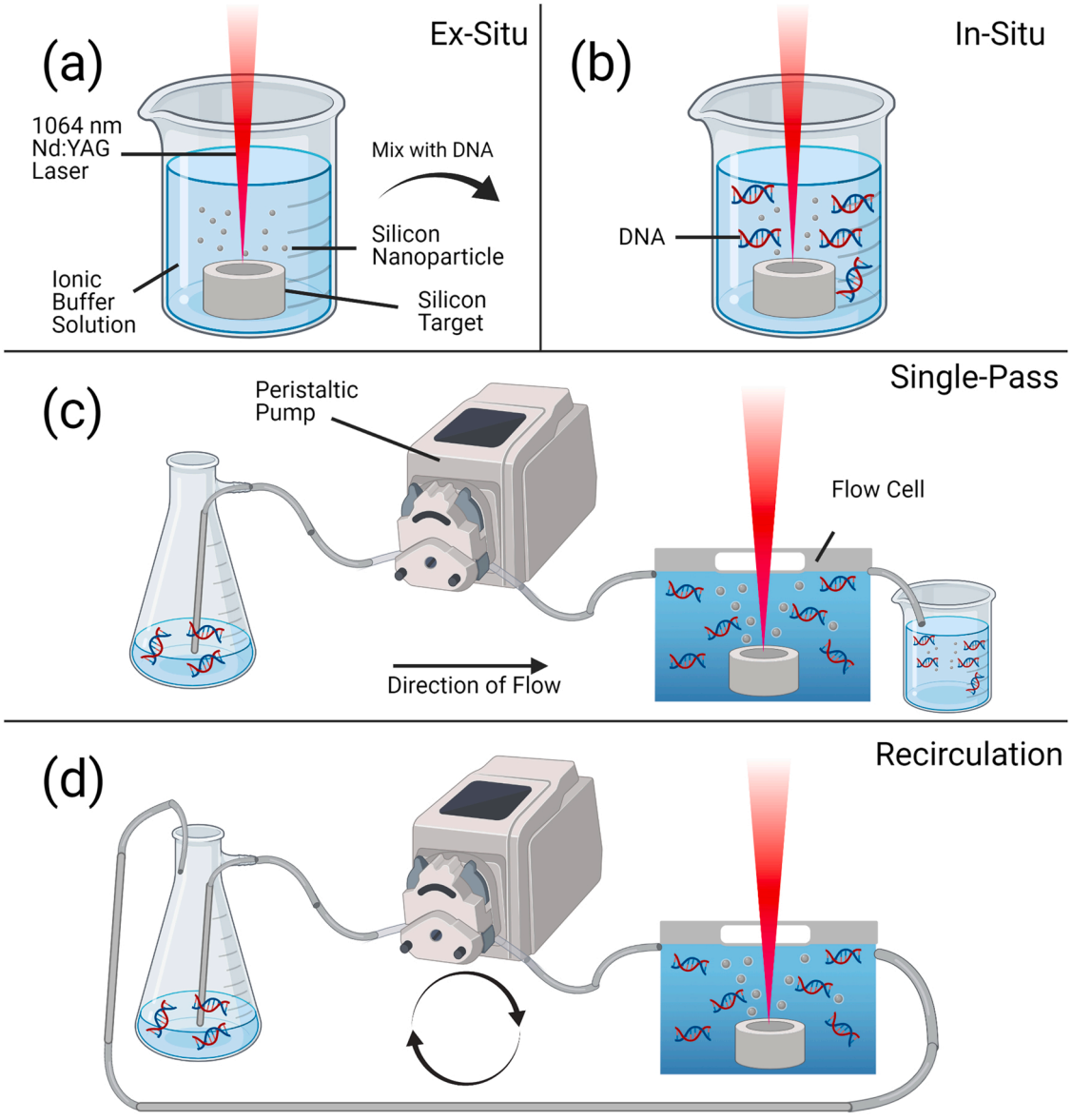

Fig. 1. Schematic diagram of the different PLAL setups (a) Static ex-situ ablation. The target was submerged in only the ionic buffer solution and then mixed with DNA after ablation. (b) Static in-situ ablation. The target was submerged in an ionic buffer solution containing DNA (c) Single-pass flow ablation. The target was placed within a flow cell and the DNA-buffer solution was passed over the target a single time. (d) Recirculatory flow ablation. The target was placed within a flow cell and the DNA buffer-solution was passed over the target multiple times. Created with BioRender.com.

respective pure solvent spectra were recorded for comparison.

The colloid concentration was determined using UV-Vis spectroscopy [Biochrom Libra S22 UV/Vis Spectrophotometer] and gravimetric analysis of the cleaned silicon target before and after ablation. The spectrometer scan range was 220–800 nm, moving in 0.5 nm intervals. The recorded UV-Vis spectra were corrected for the solvent (DI Water, Buffer, or DNA-Buffer) contribution.

2.3. DNA binding characterization

For DNA binding characterization, a 1 mL aliquot of the colloid was centrifuged [Eppendorf Centrifuge 5430R] at 17,500 RPM and 20 °C for 20 min. These parameters allowed for complete separation of unbound DNA from the DNA-SiNP conjugates. The DNA functionalized SiNPs formed a pellet, while unbound DNA remained in suspension. Fluorescence spectra of the supernatant was measured via fluorescence spectroscopy allowing for the quantification of unbound DNA. By measuring the DNA of the colloid before centrifugation and subtracting the DNA measurement of the separated supernatant, an estimate of the percentage of functionalized SiNPs could be acquired. The binding efficiency errors are calculated by propagating the standard deviations of both the colloid and supernatant fractions, with "n" denoting the number of measurements taken.

DNA binding was measured using the Quant-iT PicoGreen dsDNA Assay [Life Technologies, Dublin, Ireland]. This dye uses fluorophores which will only bind to double-stranded DNA, which not only serves as a measurement for the DNA, but it also showed that the DNA did not become denatured during the ablation process. The dye was made up of a 200-fold dilution of the concentrated dimethyl sulfoxide solution in the 1x TE buffer supplied with the PicoGreen Assay kit [10 mM Trisaminomethane-HCl, 1 mM Ethylenediaminetetraacetic acid, pH 7.5], within reflective foil covered plastic containers. The assay was performed in a 96-well plate [Nunclon MicroWell, Sigma Aldrich], where a 1:1 aliquot of sample and dye (40 μL each) was placed in each well. Other wells were filled with 40 μL of both buffer and dye to serve as the background for correction. The plate was covered in reflective foil, and the samples and dye were left to incubate for 5 min before being placed in a spectrofluorometer [Tecan Safire 2, Tecan Group Ltd, Switzerland]. The excitation (λ_{ex}) and emission (λ_{em}) wavelengths were 480 nm and 520 nm, respectively.

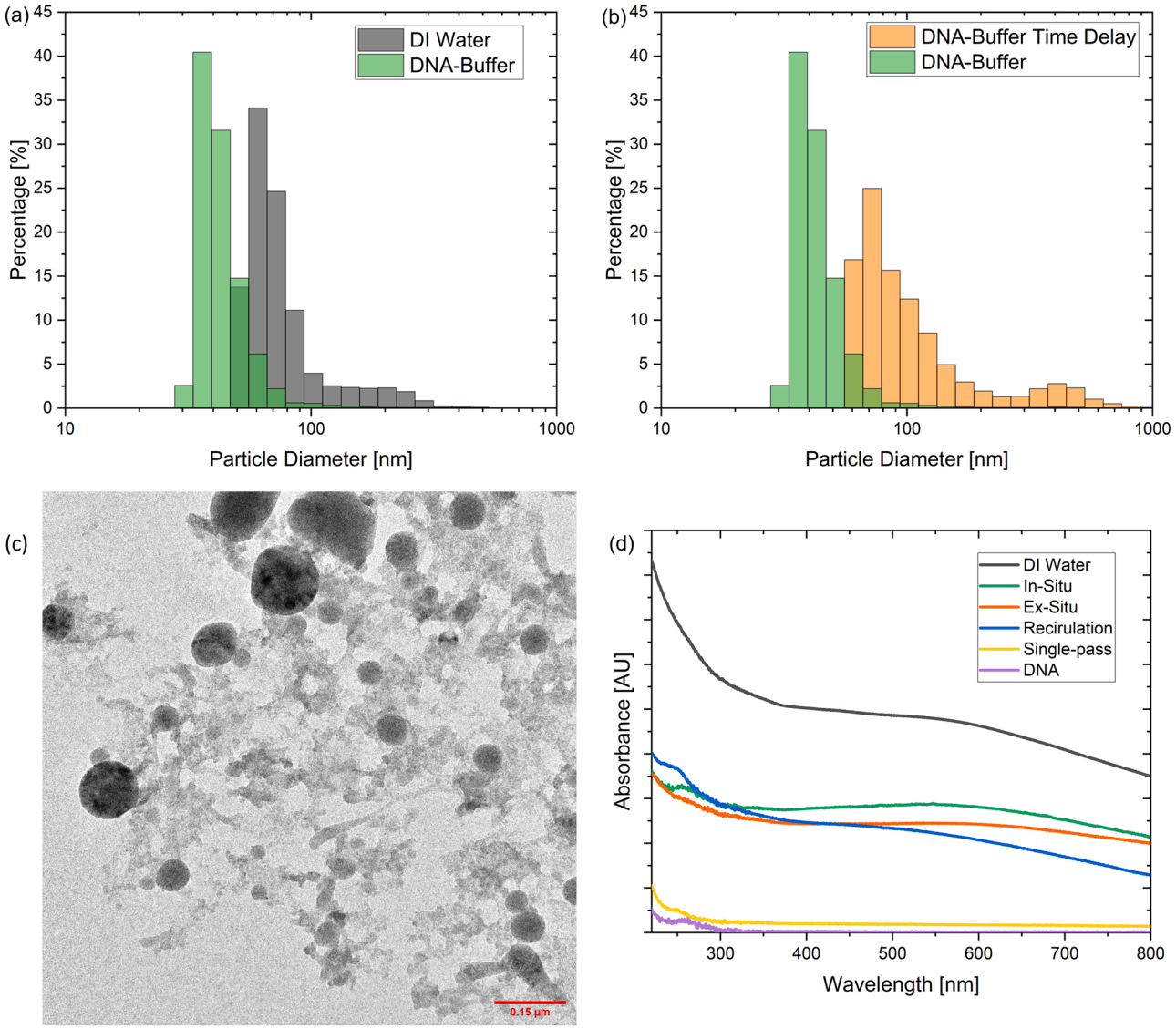

Fig. 2. (a) Size distribution of SiNPs with largest peaks between 25 and 100 nm in diameter (n = 3) (b) Size distribution of SiNPs produced in DNA-Buffer, showing the agglomeration effects over time due to a time delay between synthesis and measurement (c) TEM image of SiNPs with 150 nm scale bar (d) UV-Vis spectra for SiNPs ablated under each flow condition for 20 min in 2 μg/mL of DNA alongside a pure DNA sample for reference. (n = 3) (Single-pass ablations are time independent and DI Water and Ex-Situ ablations are free from DNA).

3. Results & discussion

3.1. SiNP characterization

By DLS measurement, ~98% of SiNPs produced in the DNA-Buffer solution were within the size range of 25–100 nm, with a peak distribution at 40 nm, when measured shortly after synthesis. SiNPs produced in DI water were larger (peak = 60 nm), with a broader, long-tailed size distribution (Fig. 2.a). This DLS measurement is supported by a TEM image of SiNPs produced in DI water (Fig. 2.c) showing the nanoscale dimensions of spherical SiNPs. It is expected that SiNPs made in DNA-buffer would be smaller compared with those in DI water due to size capping effects of ligands during PLAL. This size-capping phenomenon has been demonstrated numerous times using biomolecules [16, 34–39]. While it is expected that SiNPs produced in DNA would exhibit ultrasmall diameters (5–20 nm), the larger apparent sizes seen in the DLS measurement may be due to the fact that the hydrodynamic diameter of the conjugated particles is measured, rather than a direct measurement of the core NP diameter. DNA ligands on the surface of the core NPs may also be interfering with the measurement, indicating a larger particle size. It is well known that hydrodynamic-based measurement techniques such as DLS report larger particle diameter sizes compared with direct imaging techniques such as TEM for conjugated and unconjugated NPs, as reported widely in literature [16,18,36, 40–42]. Agglomeration effects for SiNPs made in DNA were also directly observed. Time delays between synthesis and measurement of these samples lead to distinct changes in the measured sizes, shown in Fig. 2.b. NPs have a tendency to agglomerate over time, so for a true size comparison, the time delay between synthesis and measurement must be kept constant for all NP samples [18]. By performing synthesis in DNA solution, followed by immediate DLS measurement, a reduction in size beyond that of SiNPs produced in DI water was observed. Thus size capping effects of the DNA ligands were observed. However, the fact still remains, that DLS measurement doesn't indicate the diameter of the core SiNP, but rather its hydrodynamic diameter.

Furthermore, it was observed that the peak diameter of DNA-functionalized SiNPs increased with ablation time during recirculatory ablation testing (Fig. S1, supplementary). Twenty-minute recirculatory ablation tests reported DNA-functionalized SiNPs with an hydrodynamic of 80–150 nm, whereas 60-min ablations produced NPs with diameters of 100–500 nm. Bare metallic NPs size reduction with increased ablation time under recirculatory flow conditions has been reported previously [43]. The authors reported that the size reduction was due to reirradiation of the metallic particles, however DNA functionalized NPs have been observed to perform differently in this work. The hydrodynamic size increase observed (Fig. S1, supplementary) may be due to increased DNA binding on the surface of the SiNPs, leading to larger particle diameters measured by the DLS. Indeed, increased DNA binding with ablation time is observed in this work (Fig. 6). Additionally, the influence of chaotropic salts and/or DNA which may cause SiNPs to aggregate more quickly over longer time durations cannot be ruled out.

Ultrasmall SiNPs are known to have λ_{ex} and λ_{em} in the near UV and blue-green regions of electromagnetic spectrum, respectively, which is indicated by the steepness of the shoulder seen in the UV-Vis absorption spectra (Fig. 2.d) [44]. Since we were using PicoGreen fluorophores (λ_{ex} = 480 nm, λ_{em} = 520 nm), we first verified that the fluorophores did not bind to the SiNPs on their own and that the SiNPs themselves are not fluorescent at these wavelengths given that the shoulder occurs around the emission-excitation band (Fig. 2.d). The UV-Vis absorption spectra in Fig. 2.d shows the clear presence of DNA and SiNPs (or lack thereof) in the colloids, indicated by the characteristic DNA absorption peak at 260 nm and the broadband absorption of all wavelengths associated with SiNPs. While the UV-Vis data shows qualitatively the presence of SiNPs and functionalized DNA, it cannot be used to quantify the functionalization as one cannot distinguish the relative contributions from the DNA and SiNPs to the 260 nm peak of the colloid. Therefore, we used fluorescence spectroscopy for the quantification of captured DNA as it provides a measurement of only DNA and not the SiNPs.

Composition and crystallographic data for the produced SiNPs were obtained using XRD, FTIR, and EDX. The XRD data (Fig. 3.a) for SiNPs in water indicates a polycrystalline deposit, with peaks in excellent agreement with theoretical angles for the cubic structure silicon crystal planes (JCPDS 27–1402), typical for SiNPs in literature [45,46]. The SiNPs in DNA solution similarly show the Si (111) peak (which is expected to be the most intense peak in a powder pattern), albeit with a significantly reduced intensity. This reduced intensity may be due to the smaller particle sizes/volumes, due to the size capping of ligands, since XRD intensities are proportional to volume [47]. The two other peaks present in the DNA-SiNP spectra are likely due to some leftover chloride salts from the ionic buffer solution. Given the reduced (111) peak intensity, the (220) and (311) peaks are likely below the limit of detection. These XRD data confirm the presence of crystalline Si material in the NPs, as the core of the SiNPs. FTIR data (Fig. 3.b) shows a broad and distinct peak at 1104 cm^{-1} and 1086 cm^{-1} for SiNPs in DI water and DNA, respectively. These peaks correspond to the characteristic asymmetric stretching vibrations of the Si–O–Si bond of silica [45,48,49]. We also see a smaller peak in the DNA SiNP spectra at 966 cm^{-1}, potentially indicative of the Si–OH bond [45]. However, this could be a shifted peak from the DNA spectra as we see a similar peak around 944 cm^{-1}. These latter data confirm the presence of silica in the NPs, and the combined

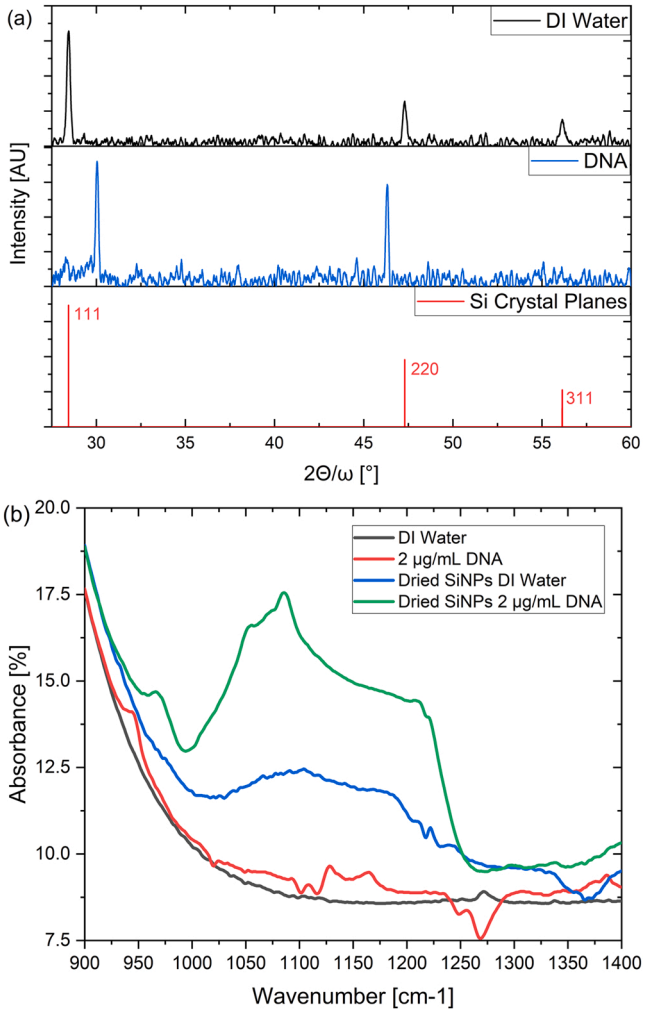

Fig. 3. (a) XRD patterns obtained for SiNPs made in DI water and DNA alongside the locations of theoretically calculated silicon crystal planes. (b) FTIR Spectra obtained for the same SiNP samples alongside theirrespective solvents.

XRD and FTIR results provide strong evidence of silicon-core, silica-shell SiNP structures, which is in agreement with previous reports of SiNPs made by PLAL [16,50]. This oxide shell is of particular importance as previous groups have discovered that the binding of DNA to SiNPs during PLAL occurs at defect sites in the silica layer [16], which is likely to also be the functionalization mechanism for our NPs. Using Raman scattering, the chemical bonding between SiNPs and the DNA backbone was identified as a stretching vibration of Si–C/Si–CH (H_xC_{4-x}-SiO_x, x = 1–3). These results are supported by EDX analysis, which show the predominance of silicon and oxygen in the SiNP samples. The DI water SiNPs showed an atomic percentage of (82.08 ± 8.41%) silicon and (17.99 ± 8.42) oxygen, with DNA-SiNPs containing (55.12 ± 27.95%) silicon and (44.76 ± 27.36%) oxygen. The results and corresponding SEM images can be found in the Supplementary data (Figs. S2-S7, Table S1). The DNA-SiNPs also contained signals from chlorine from the ionic buffer but, in both solutions, silicon and oxygen signals dominated the emissions.

While Fig. 2 shows the difference in concentration for each method during a common 20-min ablation, the differences in productivity and efficiency with time for each method is illustrated in Fig. 4. Single-Pass concentrations were time independent and not calculated gravimetrically due to the unmeasurable differences in weight after such short ablations in the more viscous DNA-Buffer, as well as the large volumes required to perform experiments for such a time that the weight difference could be measured.

The characterization of SiNP concentrations in various liquids under static and flow conditions can be seen in Fig. 4.a. We can see the curve quickly plateauing due to shielding of the target by the ablated species after around 10 min in both static ablations, whereas dynamic flow ablation shows a close to linear relationship over the one-hour region tested, demonstrating a key advantage of the recirculatory set-up. It takes longer for the plateau to develop in the buffer compared to deionized (DI) water due to their relative viscosities. The buffer is much more viscous than DI water, which reduces the ablation efficiency [51]. Therefore, it takes longer to synthesize enough SiNPs to shield the target from the laser beam. This is further shown by the similarities of static and dynamic ablation in buffer (& DNA buffer). They remain quite similar and linear up until ~20 min, at which point the SiNPs begin to significantly interact with the laser. This plateauing effect is comparable to previously published findings [17]. Under static conditions the SiNPs remain within the line of sight of the laser and shield the target, whereas under dynamic flow they move away from the target surface allowing a continuing and linear increase of ablation products with time. Single-pass SiNP concentrations are constant regardless of ablation time due to the flushing nature of the technique, which has been previously characterized by Freeland et al. [17]. The relative concentrations can be visualized by the UV-Vis data in Fig. 2.d.

3.2. DNA functionalization

Initially, we investigated the functionalization efficiency when ablating silicon in solutions of varying DNA concentrations for 20 min, which can be seen in Fig. 5. We achieved significant binding of DNA to the SiNPs across the range of concentrations tested, with a maximum average efficiency of 52% achieved with the 2 μg/mL DNA concentration using the static in-situ set-up. The ex-situ results (Fig. 1.a) also showed significant binding across the same range of DNA concentrations, however, with far more variation compared to the in-situ (Fig. 1.b) results. Fig. 5 suggests that the SiNPs become saturated as the DNA concentration increases. The in-situ method exhibits higher binding efficiency at lower concentrations whereas the ex-situ method exhibits slightly higher binding efficiency at higher concentrations, though the repeatability of the technique decreases at the highest concentration of DNA (100 μg/mL). The results at 2 μg/mL suggest that the state of the NPs either during or immediately after ablation (in-situ) is more conducive to functionalization than long after ablation which is the case

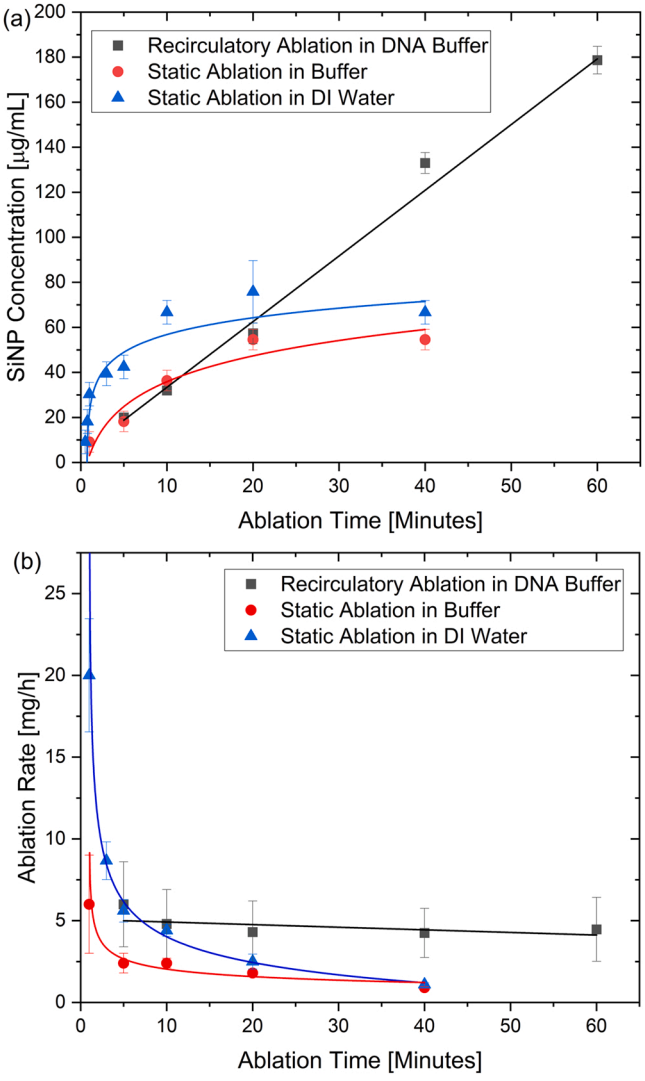

Fig. 4. (a) SiNP colloid concentration vs time for varying liquid media under static and flow conditions. Both static ablations plateaus in growth whereas the recirculatory flow shows a linear relationship with a slope of 2.9999 and R^2 = 0.9918. (n = 3 ± SD) (b) Ablation Rate vs Ablation Time for the same data showing the increased productivity of PLAL under dynamic flow conditions.

in ex-situ conditions. The comparable binding efficiencies at higher concentrations are likely due to the sheer amount of DNA available to bind. Here there is no need for the added benefits of laser ablation, as the surfaces become quickly saturated with no more available binding sites via physical adsorption under chaotropic conditions. Silica surfaces are terminated with silanol groups which provide active positions for DNA under these conditions, allowing relatively large ex-situ binding to occur [29], [52]. The in-situ produced SiNPs, therefore, benefit from this binding mechanism post-ablation combined with the aforementioned chemical bond between SiNP and DNA backbone of Si–C/Si–CH during/shortly after ablation. The 20 and 100 μg/mL samples were diluted to 2 μg/mL prior to measurement, as they were previously outside the linear detection range of the PicoGreen dye (a calibration curve from 2 to 2000 ng/mL was generated to validate this linearity). Significant ex-situ binding is to be expected at these large concentrations, given silicon's desirable surface properties for physical adsorption of proteins and DNA/RNA [29,53]. In addition, our in-situ binding efficiency of 29.1% at 20 μg/mL is comparable to the work of Bagga et al., who achieved a binding efficiency of 26% of Protein A from *Staphylcocous aureous* when ablating in 25 μg/mL [54].

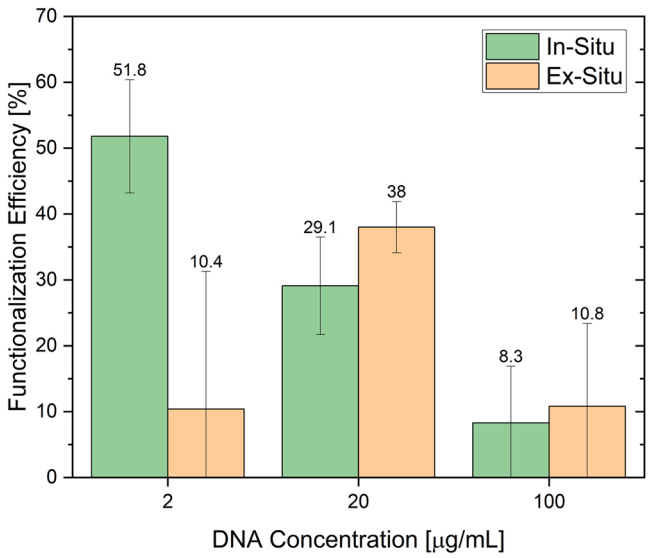

Fig. 5. Normalized fluorescence intensity of the DNA captured at each DNA solution concentration (2, 20 and 100 µg/mL). The in-situ data shows the efficiency of capture is highest at low concentrations of DNA and that the SiNPs are becoming saturated with DNA at high concentrations. The ex-situ method shows large variations in efficiency at the high and low DNA concentrations. (n = 9 for 2 µg/mL and 100 µg/mL and n = 3 for 20 µg/mL).

In order to improve upon these binding efficiencies further, we incorporated the recirculatory dynamic flow conditions of the design from Freeland et al. [14] (Fig. 1.c & d). The dynamic flow cell setup not only provides higher SiNP ablation efficiency/productivity, but enhances mixing/interaction mechanisms which we hypothesised could further improve DNA-SiNP binding.

Fig. 6 shows the binding efficiencies for recirculatory flow (Fig. 1.d) after five ablation times. We investigated lower ablation times compared to the static ablation methods due to the increased volumes and NP productivity, as well as the enhanced mixing in the flow which could potentially increase binding on shorter timescales. It was expected that as SiNP concentration increases, the DNA binding efficiency would follow, due to the addition of free SiNP surfaces available for functionalization. This trend is broadly illustrated in Fig. 6, however the 10-min

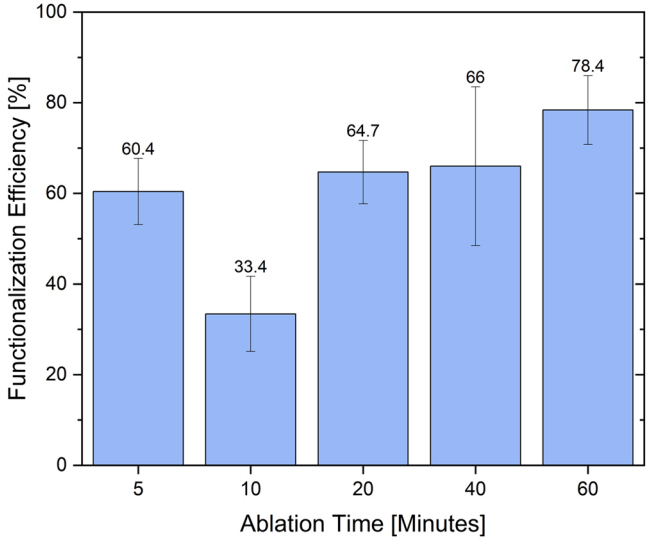

Fig. 6. Binding efficiency vs ablation time for 2 µg/mL DNA under dynamic flow conditions in recirculatory flow. We can see a small increase in binding efficiency as we increase the ablation time. (n = 9).

ablation shows lower binding efficiency compared with 5-min and 20-min ablations, even though the SiNP concentration has been seen to increase linearly (Fig. 4.a). This indicates that either the single-step functionalization has not reached a steady state of operation or factors including localized DNA aggregation, or the heat of the recirculated colloid and plasma plume stabilizes after 10-min recirculatory ablation. In either case, we have significantly increased the binding efficiencies compared to the traditional static PLAL, going from 52% (for the static system) to 65% (for the recirculatory system) binding efficiencies for the same ablation time.

The small relative increase in binding efficiency vs time for each recirculatory ablation suggests an inhibiting factor limiting binding efficiency increase, such as electrostatic repulsion within the DNA itself and between SiNPs due to their strong zeta-potentials [13]. However, we decided to investigate the thermal activity of the system by placing a thermocouple probe on the surface of the silicon target during a 60-min ablation, to capture real-time temperature data in order to better understand the unexpected results obtained for 10-min ablations. We drilled a hole through the underside of the flow cell and threaded a thermocouple wire through it. The wire was held in place with, and the hole filled by, an epoxy-based glue. This ensured that the flow cell remained watertight, and that the thermocouple would not move significantly during the experiment. Due to the lateral positioning of the thermocouple (away from the inlet and outlets), the flow was not impeded by the thermocouple, and its presence did not induce bubble generation above the silicon target. The beam was positioned such that the nearest point on the ablation site was 0.6 mm away from the thermocouple (see Fig. 7.b). Corresponding infrared images were taken with an FLIR One Pro camera, but the camera's inability to measure through glass resulted in temperature measurements of the borosilicate glass laser window rather than the ablation site itself.

The results in Fig. 7.a show the temperature increases initially but starts to plateau after ~30 min, but with a recurring pattern with a 2-min period shown in greater detail in the inset. The thermocouple probe was sampled once every second, but to further understand the periodic pattern observed, we repeated the first two minutes of the experiment with 0.24 s delay between measurements (which was the smallest obtainable delay) to obtain a more accurate representation of the temperature fluctuations. We observed intense local changes in temperature due to the laser's position relative to the thermocouple. The peaks and troughs are due to the spiral coming closer to, and further away, from the thermocouple. We see the highest temperature differences initially, as the spiral diameter/circumference is at its largest. The time difference between the first two peaks is 6.7 s, and the maximum circumference of our spiral pattern is 14.2 mm. Our laser travels at 2 mm/s which means it would take 7.1 s to complete one full rotation, so we expect to see the first peak after this time, consistent with the measured data. Slight discrepancies are likely due to the sampling intervals not exactly lining up with positions closest or furthest from the thermocouple. Additionally, we do not see the first outermost spiral as this occurs during the initial rise in temperature after ~1 s, just prior to the cyclical pattern. We also see that the not only do the temperature differences decrease over time, but so do the periods between peaks. This is due to the decreasing spiral diameter/circumference, meaning the difference in the distance to the thermocouple probe along all points of the spiral also decreases. A smaller circumference means less distance and therefore time, to make a full revolution, and so we see the period decreases to 0.5 s before the smaller sampling measurements were stopped.

We see on the one second sampling data that the temperature pattern approximately converges to a final value without noticeable peaks and troughs as the spiral radius reaches zero. Thereafter the spiral pattern resets to the maximum 4.5 mm diameter and the cycle repeats again. While these results did not help definitively establish the cause of our 10-min ablation result, we believe these results to be beneficial to others in the field, as the dramatic temperature differences on a macroscopic scale could warrant more studies on a micro/nanoscopic scale.

Another important point to note is the adapted approach required to

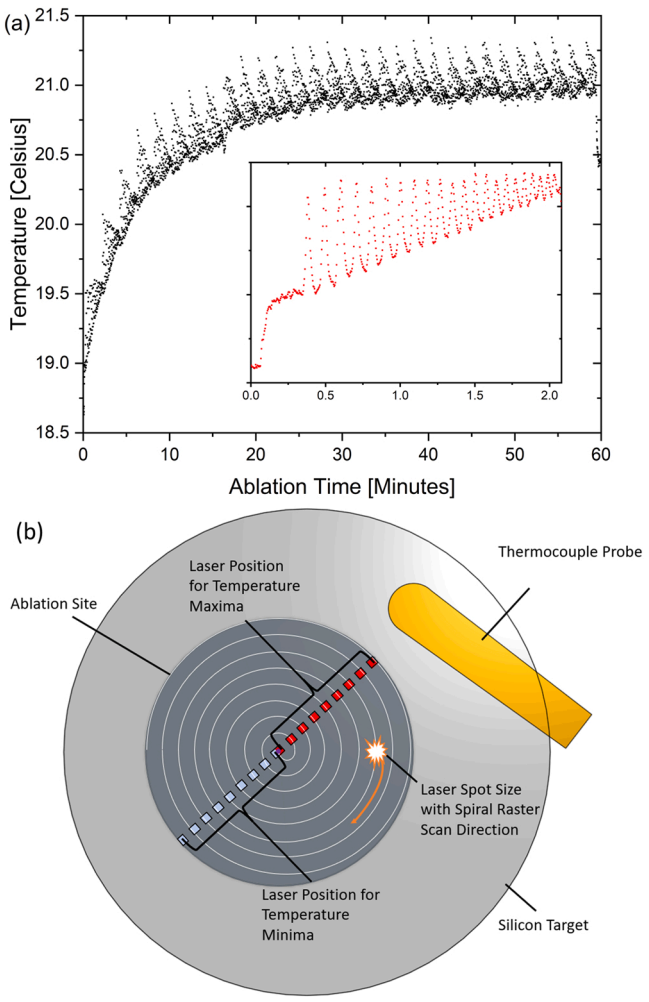

Fig. 7. (a) Temperature of the solution adjacent to the ablation site during a 60-min recirculatory ablation in DNA-Buffer with one second sampling (Inset: first two minutes of the ablation with faster, 0.24 s sampling). (b) AutoCAD illustration of the ablation site showing the position of the thermocouple to scale. The silicon target diameter is 8.28 mm.

measure the binding efficiency for the longer ablation times of the dynamic flow cell tests compared to the static tests. It was assumed that when ablating in 2 μg/mL of DNA, the collected colloid still contained 2 μg/mL DNA but as a combination of bound and unbound DNA. The colloid fluorescence values were compared to the fluorescence of the pure 2 μg/mL DNA solution to ensure this was the case. However, it was found that the colloids of the 60-min ablations displayed only ~25% of the pure DNA fluorescence. This is believed to be due to a combination of the greatly increased SiNP concentration, and the perceived lack of stability of SiNPs at this higher ablation time. SiNPs are remarkably stable in DI water and can remain in suspension for months, whereas they are noticeably less stable in DNA buffer and fall out of suspension in a matter of weeks. The SiNPs made during the dynamic 60-min recirculatory ablation fell out of suspension within the hour, indicating a drastically reduced and almost non-existent stability. It is believed that the SiNPs falling out of suspension and agglomerating as macroparticles may cover or hide DNA rather than become functionalized by the DNA, making it undetectable. This may also block the binding sites for the PicoGreen fluorophores, resulting in the lower signals. Evidence to support these claims is shown in Fig. 8. Therefore, the recirculatory flow supernatants were subtracted from the pure DNA fluorescence rather than their corresponding colloid fluorescence values.

Fig. 9 shows the binding efficiencies during single-pass (Fig. 1.c) ablation for three different flow rates. We see the largest average binding efficiency of 22% at 40 mL/min, with the average efficiencies decreasing with flow rate. This is expected as the slower the flow is above the ablation site, the larger the interaction time for DNA-SiNP interactions. Slower flow rates produce higher NP concentrations, but lower productivity compared to higher flow rates. For a given volume of liquid, as you decrease the flow rate you consequently prolong the ablation time, resulting in a denser colloidal solution as you ablate for longer in the same volume. Therefore, while higher flowrates are ideal for producing large volumes of pure colloids, we clearly see here that lower flowrates are required for higher binding efficiencies.

However, each result displays notably large error bars, especially when compared to the previous ablation methods used in this investigation. This method can be loosely compared to the ex-situ binding, in that there is a short and somewhat random mixing/interaction between DNA and SiNPs, leading to large inconsistencies in binding efficiencies. We therefore believe that this method is optimized for the processing of pure colloids, but that more work is need in terms of the investigation of the generation of functionalized colloids. The flow rate range tested correspond to the maximum and minimum flow rates that could be achieved without introducing bubbles into the system. Bubbles significantly impact colloid generation and should be avoided at all costs. The flow system is stable and will not generate bubbles within these flow rates when using the ionic buffer, with the range being dependent on the solvent used.

Lastly, as shown in Fig. 10, we can clearly see that recirculatory ablation achieves the highest degree of functionalization. While this efficiency was increased by ablating for 60 min, the aforementioned stability issues require further investigation. We achieved a maximum average efficiency of 78% when ablating in the flow cell, which is much greater than the 52% achieved with the in-situ method, the 22% achieved with the single-pass method, and the 10% achieved with the ex-situ method. There are also much smaller error bars associated with the recirculatory and batch/static in-situ measurements, leading us to believe these are more consistent techniques. This was hypothesized to be due to the low DNA to SiNP ratio alongside the much-longer mixing time of these method. During the in-situ and recirculatory tests, the binding process essentially occurs over 20 min and 5–60 min respectively, while the silicon is being ablated, compared to the approximately 10-s hand mixing binding method of the ex-situ test, and the short interaction time during single-pass ablations. The smaller number of steps taken in the in-situ test further reduces the possible errors as the ex-situ method has significantly larger error bars. The dynamic recirculatory ablation having a larger efficiency than the static in-situ is to be expected given the increased ablation efficiency and mixing effects of the recirculatory flow conditions. Preliminary tests with lower concentrations (0.5 μg/mL) have also been carried out, which show close to 100% binding efficiency (99.6 ± 6.7%) of the DNA in solution, which we believe to be the highest reported functionalization efficiency by any

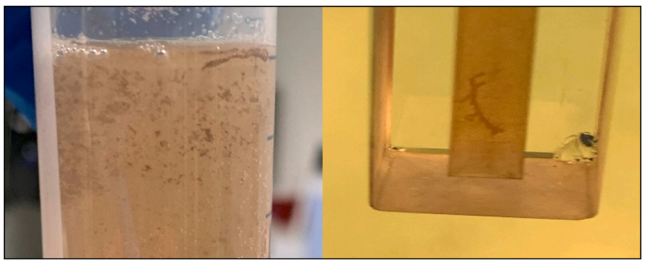

Fig. 8. (Left) SiNPs binding together along long strands of DNA, (Right) SiNP instability after 60-min ablation indicated by visible agglomerated macroparticles of Si alongside SiNP coated DNA strands.

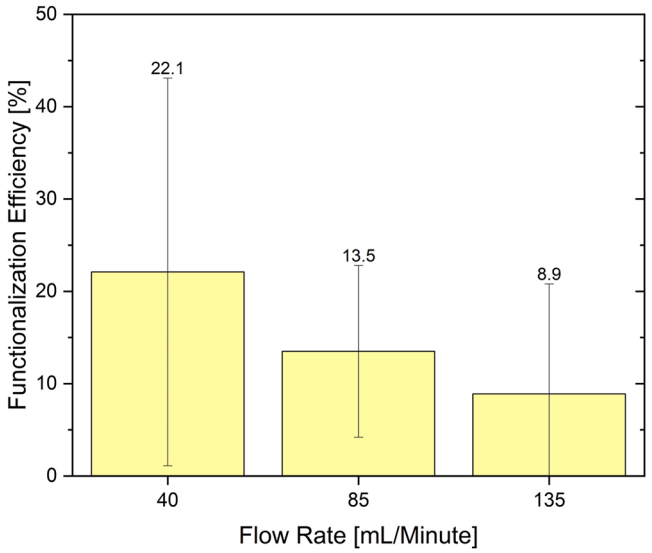

Fig. 9. Binding efficiency vs flow rate for 2 μg/mL DNA under single-pass flow conditions. We can see a small but clear decrease in binding efficiency as we increase the flow rate. (n = 9).

variation of the PLAL technique. This preliminary data suggests that further explorations may be worthwhile in this concentration range. Our results show significantly higher binding efficiencies compared to previous reports of in-situ DNA functionalization at similar concentrations, with previously reported maximum efficiencies of 20% for unmodified DNA binding to SiNPs [16], and 40.3% efficiency for DNA modified with thiol for improved binding to gold NPs [42]. There have been reports of very high binding efficiencies (over 90%) for some other types of modified ligands and NPs in flow systems, but our results for binding efficiencies appear to be the highest reported for unmodified DNA binding to SiNPs [55].

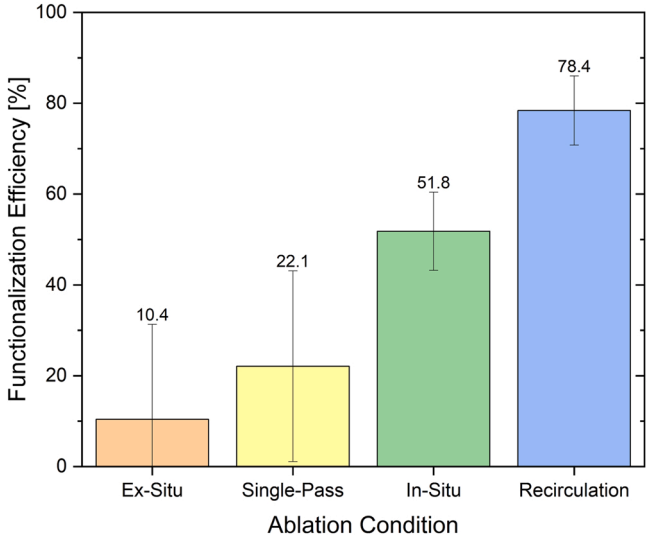

Fig. 10. Maximum binding efficiencies of each method in 2 μg/mL of DNA. (n = 9).

4. Conclusion

We have shown successful DNA binding to SiNPs under both static and dynamic flow conditions. We achieved a maximum average binding efficiency of 52% under static conditions and an increased binding efficiency of 65% under novel, recirculating flow conditions for a 20-min ablation. Increasing the ablation time to 60 min under flow, this work demonstrated a DNA binding efficiency of 78%, which is a 50% relative increase in what was achievable from static ablation while also producing significantly more functionalized NPs per unit time. By further reducing the stock DNA concentration to 0.5 μg/mL, we achieved essentially 100% binding efficiency by recirculatory ablation, the highest reported in the literature, to our knowledge.

Static ablation serves well as a mechanism for PLAL research, but the introduction of controlled recirculating flow makes the technique suitable for industrial scale production due to the large volumes and higher functionalization efficiencies that can be produced, making it a more desirable NP synthesis technique for functionalized nanomaterials.

Future work will address optimization of ablation time to determine the ideal parameters for SiNP production, stability, and functionalization, alongside investigating other biomolecules for functionalization. We also wish to demonstrate the nucleic acid capture and detection capabilities of our recirculating-flow produced functionalized nanoparticles.

Data availability statement

The data that supports the findings of this study are available upon reasonable request from the authors.

CRediT authorship contribution statement

Paul Cannon: Validation, Formal analysis, Investigation, Data curation, Writing – original Draft, Visualization, Funding acquisition, **Brian Freeland:** Conceptualization, Methodology, Resources, Writing – review & editing, Supervision, **Margaux Jaquiery:** Validation, Formal analysis, Investigation, **Enda McGlynn:** Writing – review & editing, Supervision, Funding acquisition, **Jennifer Gaughran:** Conceptualization, Methodology, Resources, Writing – review & editing, Supervision, Project administration, Funding acquisition.

Declaration of Competing Interest

The authors declare that they have no known competing financial interests or personal relationships that could have appeared to influence the work reported in this paper.

Acknowledgments

The research conducted in this publication was funded by both the Irish Research Council under the Government of Ireland Postgraduate Scholarship Programme [grant number: GOIPG/2021/379] and also Dublin City University's School of Physical Sciences, Ireland.

The authors would like to thank I-Form, the Science Foundation Ireland Research Centre for Advanced Manufacturing, for the use of their laser system, and Ms. Mandy Juillerat and Dr. Michal Dabros from the School of Engineering and Architecture, HES-SO University of Applied Sciences and Arts Western Switzerland, Bd de Pérolles 80, CH-1700 Fribourg, Switzerland for TEM imaging.

The FTIR measurements were carried out at the Nano Research Facility in Dublin City University which was funded under the Programme for Research in Third Level Institutions (PRTLI) Cycle 5. The PRTLI is co-funded through the European Regional Development Fund (ERDF), part of the European Union Structural Funds Programme 2011–2015.

Appendix A. Supporting information

Supplementary data associated with this article can be found in the online version at doi:10.1016/j.colsurfa.2022.129217.

References

[1] M.A. Dineva, L. Mahilum-Tapay, H. Lee, Sample preparation: a challenge in the development of point-of-care nucleic acid-based assays for resource-limited settings, in: Analyst, vol. 132, Royal Society of Chemistry, 2007, pp. 1193–1199.
[2] K. Mullis, F. Faloona, S. Scharf, R. Saiki, G. Horn, H. Erlich, Specific enzymatic amplification of DNA in vitro: the polymerase chain reaction, Cold Spring Harb. Symp. Quant. Biol. 51 (1) (1986) 263–273.
[3] P. Yager, G.J. Domingo, J. Gerdes, Point-of-care diagnostics for global health, Annu. Rev. Biomed. Eng. 10 (2008) 107–144.
[4] X. Zhao, R. Tapec-Dytioco, W. Tan, Ultrasensitive DNA detection using highly fluorescent bioconjugated nanoparticles, J. Am. Chem. Soc. 125 (38) (2003) 11474–11475.
[5] D. Paolino, et al., Targeting the thyroid gland with thyroid-stimulating hormone (TSH)-nanoliposomes, Biomaterials 35 (25) (2014) 7101–7109.
[6] P. Singh, S. Pandit, V.R.S.S. Mokkapati, A. Garg, V. Ravikumar, I. Mijakovic, Gold nanoparticles in diagnostics and therapeutics for human cancer, Int. J. Mol. Sci. 19 (7) (2018).
[7] G. Ajnai, A. Chiu, T. Kan, C.C. Cheng, T.H. Tsai, J. Chang, Trends of gold nanoparticle-based drug delivery system in cancer therapy, J. Exp. Clin. Med. 6 (6) (2014) 172–178.
[8] Y. Uludag, G. Köktürk, Determination of prostate-specific antigen in serum samples using gold nanoparticle based amplification and lab-on-a-chip based amperometric detection, Microchim. Acta 182 (9) (2015) 1685–1691.
[9] M. De, P.S. Ghosh, V.M. Rotello, Applications of nanoparticles in biology, Adv. Mater. 20 (22) (2008) 4225–4241.
[10] P.G. Jamkhande, N.W. Ghule, A.H. Bamer, M.G. Kalaskar, Metal nanoparticles synthesis: an overview on methods of preparation, advantages and disadvantages, and applications, J. Drug Deliv. Sci. Technol. 53 (2019).
[11] G.L. Bratthauer, The avidin-biotin complex (ABC) method and other avidin-biotin binding methods, Methods Mol. Biol. 588 (2010) 257–270.
[12] W. Wang, D.W. Pang, H.W. Tang, Sensitive multiplexed DNA detection using silica nanoparticles as the target capturing platform, Talanta 128 (2014) 263–267.
[13] K. Bagga, et al., Laser-assisted synthesis of ultrapure nanostructures for biological sensing applications, Proc. SPIE (2016) 99280O.
[14] B. Freeland, R. McCann, G. Alkan, B. Friedrich, G. Foley, D. Brabazon, Stable nano-silver colloid production via Laser Ablation Synthesis in Solution (LASiS) under laminar recirculatory flow, Adv. Mater. Process. Technol. (2020) 1–9.
[15] D. Zhang, B. Gökce, S. Barcikowski, Laser synthesis and processing of colloids: fundamentals and applications, Chem. Rev. 117 (5) (2017) 3990–4103.
[16] R. Intartaglia, et al., Bioconjugated silicon quantum dots from one-step green synthesis, Nanoscale 4 (4) (2012) 1271–1274.
[17] B. Freeland, R. McCann, G. Foley, D. Brabazon, High-efficiency generation of nanomaterials via laser ablation synthesis in solution with in-situ diagnostics for closed-loop control, Synth. Photon. Nanosc. Mater. 11269 (2020) 53–58. ⟨https://doi.org/10.1117/12.2545878⟩.
[18] S. Barcikowski et al., Handbook of Laser Synthesis of Colloids, 1st ed. Essen, 2016.
[19] V. Amendola, M. Meneghetti, What controls the composition and the structure of nanomaterials generated by laser ablation in liquid solution?, in: Physical Chemistry Chemical Physics, vol. 15 The Royal Society of Chemistry, 2013, pp. 3027–3046.
[20] H. Zeng, et al., Nanomaterials via laser ablation/irradiation in liquid: a review, Adv. Funct. Mater. 22 (7) (2012) 1333–1353.
[21] B. Gökce, R. Streubel, and S. Barcikowski, Continuous multigram nanoparticle synthesis by high-power, high-repetition-rate ultrafast laser ablation in liquids, Opt. Lett. vol. 41, 7, pp. 1486–1489, vol. 41, no. 7, pp. 1486–1489, Apr. 2016.
[22] F. Waag, B. Gökce, S. Barcikowski, Ablation target cooling by maximizing the nanoparticle productivity in laser synthesis of colloids, Appl. Surf. Sci. 466 (2019) 647–656.
[23] B. Freeland, et al., Real-time monitoring and control for high-efficiency autonomous laser fabrication of silicon nanoparticle colloids, Int. J. Adv. Manuf. Technol. 114 (1) (2021) 291–304.
[24] O. Długosz, K. Szostak, A. Staroń, J. Pulit-Prociak, M. Banach, Methods for reducing the toxicity of metal and metal oxide NPs as biomedicine, in: Materials, 13, Basel, 2020, p. 279.
[25] G. Mustafa, S. Komatsu, Toxicity of heavy metals and metal-containing nanoparticles on plants, Biochim. Biophys. Acta - Proteins Proteom. 1864 (8) (2016) 932–944.
[26] J.L. Vivero-Escoto, I.I. Slowing, V.S.Y. Lin, B.G. Trewyn, Mesoporous silica nanoparticles for intracellular controlled drug delivery, Small 6 (18) (2010) 1952–1967.
[27] A. Bitar, N.M. Ahmad, H. Fessi, A. Elaissari, Silica-based nanoparticles for biomedical applications, Drug Discov. Today 17 (19–20) (2012) 1147–1154.
[28] B. Shi, Y.K. Shin, A.A. Hassanali, S.J. Singer, DNA binding to the silica surface, J. Phys. Chem. B 119 (34) (. 2015) 11030–11040.
[29] R. Boom, C.J.A. Sol, M.M.M. Salimans, C.L. Jansen, P.M.E. Wertheim-Van Dillen, J. Van Der Noordaa, Rapid and simple method for purification of nucleic acids, J. Clin. Microbiol. 28 (3) (1990) 495–503.
[30] B. Freeland, R. McCann, P. O'Neill, K. Bagga, G. Foley, and D. Brabazon, Flow-regime and laser wavelength optimization of Silicon Nanoparticle fabrication via laser ablation synthesis in solution (LASiS), in 22nd Sir Bernard Crossland Symposium, 2019.
[31] V. Amendola, et al., Room-temperature laser synthesis in liquid of oxide, metal-oxide core-shells, and doped oxide nanoparticles, in: Chemistry - A European Journal, vol. 26, Wiley-VCH Verlag,, 2020, pp. 9206–9242.
[32] P. Mercier, R. Savoie, Interaction of DNA with Silica Particles: A Vibrational Spectroscopic Study, John Wiley & Sons, Inc, 1997.
[33] F. Ahmadi, N. Jamali, R. Moradian, B. Astinchap, Binding studies of pyriproxyfen to DNA by multispectroscopic atomic force microscopy and molecular modeling methods, DNA Cell Biol. 31 (2) (2012) 259–268.
[34] F. Mafuné, J.Y. Kohno, Y. Takeda, T. Kondow, H. Sawabe, Formation of gold nanoparticles by laser ablation in aqueous solution of surfactant, J. Phys. Chem. B 105 (22) (2001) 5114–5120.
[35] G. Compagnini, A.A. Scalisi, O. Puglisi, C. Spinella, Synthesis of gold colloids by laser ablation in thiol-alkane solutions, J. Mater. Res. 19 (10) (2004) 2795–2798.
[36] S. Petersen, S. Barcikowski, In situ bioconjugation: single step approach to tailored nanoparticle-bioconjugates by ultrashort pulsed laser ablation, Adv. Funct. Mater. 19 (8) (2009) 1167–1172.
[37] S. Petersen, J. Jakobi, S. Barcikowski, In situ bioconjugation-Novel laser based approach to pure nanoparticle-conjugates, Appl. Surf. Sci. 255 (10) (2009) 5435–5438.
[38] S. Petersen, A. Barchanski, U. Taylor, S. Klein, D. Rath, S. Barcikowski, Penetratin-conjugated gold nanoparticles - design of cell-penetrating nanomarkers by femtosecond laser ablation, J. Phys. Chem. C 115 (12) (2011) 5152–5159.
[39] V. Amendola, M. Meneghetti, Controlled size manipulation of free gold nanoparticles by laser irradiation and their facile bioconjugation, J. Mater. Chem. 17 (44) (2007) 4705–4710.
[40] C.L. Sajti, A. Barchanski, P. Wagener, S. Klein, S. Barcikowski, Delay time and concentration effects during bioconjugation of nanosecond laser-generated nanoparticles in a liquid flow, J. Phys. Chem. C 115 (12) (2011) 5094–5101.
[41] C.L. Sajti, S. Petersen, A. Menéndez-Manjón, S. Barcikowski, In-situ bioconjugation in stationary media and in liquid flow by femtosecond laser ablation, Appl. Phys. A 101 (2) (2010) 259–264.
[42] J.G. Walter, S. Petersen, F. Stahl, T. Scheper, S. Barcikowski, Laser ablation-based one-step generation and bio-functionalization of gold nanoparticles conjugated with aptamers, J. Nanobiotechnol. 8 (1) (2010) 1–11.
[43] S.S. Pavithran et al., Silver and Copper nano-colloid generation via Pulsed Laser Ablation in Liquid: Recirculation nanoparticle production mode, https://popups.uliege.be/esaform21, Apr. 2021.
[44] R. Intartaglia, K. Bagga, M. Scotto, A. Diaspro, F. Brandi, Luminescent silicon nanoparticles prepared by ultra short pulsed laser ablation in liquid for imaging applications, Opt. Mater. Express 2 (5) (2012) 510.
[45] P. Sahu, D. Das, Synthesis and characterization of organic ligand capped luminescent silicon nanoparticles, Mater. Today Proc. (2022).
[46] A.Y. Kharin, Y.V. Kargina, V.Y. Timoshenko, Evolution of nanocrystal size distribution in porous silicon nanoparticles during storage in aqueous media: X-ray diffraction analysis, J. Nanopart. Res. 21 (2) (2019) 1–7.
[47] C.F. Holder, R.E. Schaak, Tutorial on powder X-ray diffraction for characterizing nanoscale materials, ACS Nano 13 (7) (2019) 7359–7365.
[48] D. Das, S. Samanta, Advanced nanocrystallinity with widened optical gap realized via microstructural control in P-doped silicon oxide thin films used as window layer in nc-Si solar cells, Mater. Chem. Phys. 243 (2020), 122628.
[49] C.O. Metin, L.W. Lake, C.R. Miranda, Q.P. Nguyen, Stability of aqueous silica nanoparticle dispersions, J. Nanopart. Res. 13 (2) (2011) 839–850.
[50] R. Intartaglia, et al., Optical properties of femtosecond laser-synthesized silicon nanoparticles in deionized water, J. Phys. Chem. C 115 (12) (2011) 5102–5107.
[51] M.R. Kalus, R. Lanyumba, S. Barcikowski, B. Gökce, Discrimination of ablation, shielding, and interface layer effects on the steady-state formation of persistent bubbles under liquid flow conditions during laser synthesis of colloids, J. Flow. Chem. (2021) 1–20.
[52] D. Knopp, D. Tang, R. Niessner, Review: bioanalytical applications of biomolecule-functionalized nanometer-sized doped silica particles, Anal. Chim. Acta 647 (1) (2009) 14–30.
[53] M.C. Coen, R. Lehmann, P. Gröning, M. Bielmann, C. Galli, L. Schlapbach, Adsorption and bioactivity of protein A on silicon surfaces studied by AFM and XPS, J. Colloid Interface Sci. 233 (2) (2001) 180–189.
[54] K. Bagga, et al., Laser-assisted synthesis of Staphylococcus aureus protein-capped silicon quantum dots as bio-functional nanoprobes, Laser Phys. Lett. 10 (6) (2013), 065603.
[55] S. Petersen, S. Barcikowski, Conjugation efficiency of laser-based bioconjugation of gold nanoparticles with nucleic acids, J. Phys. Chem. C. 113 (46) (2009) 19830–19835.